

PAPER

Oxidation feature and diffusion mechanism of Zr-based metallic glasses near the glass transition point

To cite this article: Zheng Hu *et al* 2018 *Mater. Res. Express* **5** 036511


View the [article online](#) for updates and enhancements.

Materials Research Express



PAPER

Oxidation feature and diffusion mechanism of Zr-based metallic glasses near the glass transition point

Zheng Hu¹, Xianqi Lei², Yang Wang^{3,4} and Kun Zhang^{3,4} 

¹ Science and Technology on Vehicle Transmission Laboratory, China North Vehicle Research Institute, Beijing 100072, People's Republic of China

² LNM, Institute of Mechanics, Chinese Academy of Sciences, Beijing 100190, People's Republic of China

³ Key Laboratory of Microgravity, Institute of Mechanics, Chinese Academy of Sciences, Beijing 100190, People's Republic of China

⁴ School of Engineering Science, University of Chinese Academy of Sciences, Beijing 101408, People's Republic of China

E-mail: zhangkun@imech.ac.cn

Keywords: metallic glasses, oxidation, diffusion mechanism

Abstract

The oxidation behaviors of as-cast, pre-deformed, and crystallized $\text{Zr}_{47.9}\text{Ti}_{0.3}\text{Ni}_{3.1}\text{Cu}_{39.3}\text{Al}_{9.4}$ metallic glasses (MGs) were studied near the glass transition point. The oxidation kinetics of the crystallized MGs followed a parabolic-rate law, and the as-cast and pre-deformed MGs exerted a typical two-stage behavior above the glass transition temperature (T_g). Most interesting, pre-deformed treatment can significantly improve the oxidation rate of MGs, as the initial oxidation appeared earlier than for the as-cast MGs, and was accompanied by much thicker oxide scale. The EDS and XPS results showed that the metal Al acted as the preferred scavenger that absorbed intrinsic oxygen in the near-surface region of as-cast MGs. However, a homogeneous mixed layer without Al was observed in the pre-deformed MGs. We speculated the accelerated diffusion of other elements in the MGs was due to the local increase in the free volume and significant shear-induced dilation of the local structure. The results from this study demonstrate that MGs exhibit controllable atomic diffusion during the oxidation process, which can facilitate use in super-cooled liquid region applications.

Introduction

Because of their unique mechanical and chemical properties, such as high strength and superior resistance to corrosion, Zr-based metallic glasses (MGs) have attracted great interest in recent decades [1–6]. Owing to their low viscosity in the super-cooled liquid region, they can be easily fabricated by thermo-plastic forming [7–9], and use for functional applications as catalysts of fuel cells or binding agents for heterogeneous materials [10–12]. Unfortunately, these amorphous alloys often exhibit severe degradation when used in thermal activated environments. Several studies have studied the oxidation behaviors of the MGs, but with inconsistent conclusions. Some researchers find that the oxidation resistances of MGs are superior to the crystallized state, due to the lack of grain boundaries that act as local active sites for corrosion and oxidation [13, 14]. There are many MG systems that exhibit poorer oxidation resistance than their crystalline counterparts [15–19]. The addition of adequate amounts of Al or Si in Zr-based MGs could preferentially form a protective scale, which suppress the fast-growth of other oxides and increase the inhomogeneity of the oxide layer. Alternatively, surface treatments, such as pre-compression, defect-printing, cold-rolling, or surface mechanical attrition can be performed to improve the ductility of MGs, requiring suppression of the localized strain softening caused by shear bands [20]. However, only few studies have addressed the oxidation behavior of the MGs subjected to pre-deformation, which is easily induced during manufacturing.

In this study, the oxidation kinetics of pre-deformed Zr-based MGs were investigated near the glass transition temperature (T_g) and compared to as-cast and crystalline samples. Based on the results, different diffusion mechanisms were discussed. The pre-deformed surface of MGs may act as local active sites to affect subsequent oxidation.

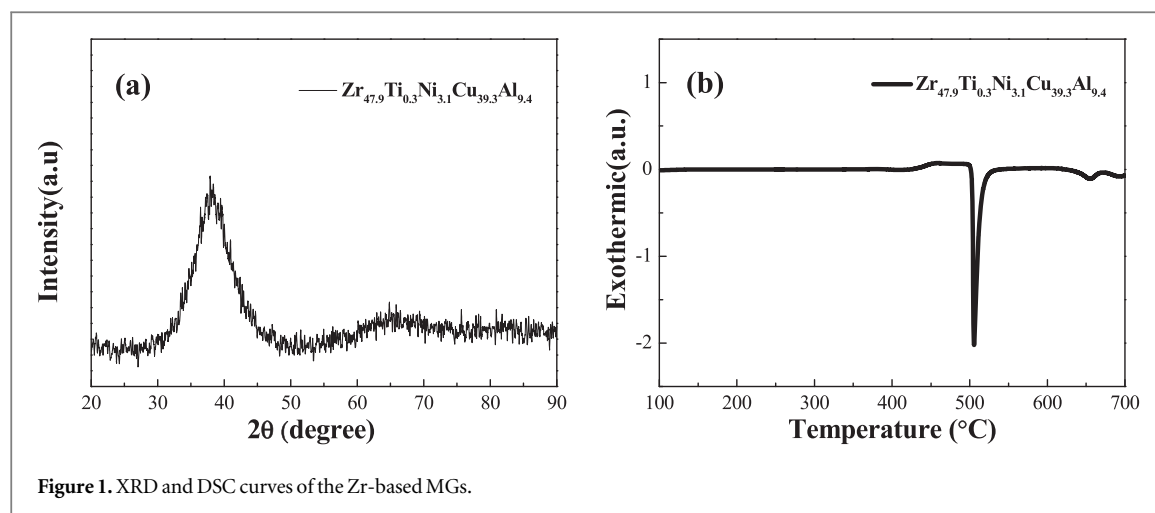


Figure 1. XRD and DSC curves of the Zr-based MGs.

Experimental procedures

The $\text{Zr}_{47.9}\text{Ti}_{0.3}\text{Ni}_{3.1}\text{Cu}_{39.3}\text{Al}_{9.4}$ ingot was prepared by arc melting a mixture of pure metals under an argon atmosphere. The alloy was re-melted several times to ensure chemical homogeneity. Cylinders of the alloys were prepared in a 5 mm shape with suction casting in a pure argon atmosphere, and then 3 mm long specimens were cut from these rods. The surfaces of the samples were mechanically polished to a mirror finish and cleaned ultrasonically. The pre-deformed specimens were prepared through depth-sensing macro-indentation over the entire surface. The crystallized samples were annealed in a vacuum at temperatures well above the crystallization temperature to ensure a fully crystalline state. Then, these as-cast, pre-deformed, and crystallized specimens were exposed to air under the thermal procedures isothermally for at least 3 h. The amorphous structure of the samples was confirmed by x-ray diffraction (XRD) using $\text{Cu K}\alpha$ radiation. The morphology of the oxidation surfaces was studied using a scanning electron microscope (SEM, JSM-6460). Energy dispersive spectroscopy (EDS) line profile analysis and x-ray photoelectron spectrometer (XPS) were performed to examine the changes of the oxidation layer in the MGs as a function of depth. The mass gain during oxidation was measured by thermo-gravimetric analysis (TGA Q50) in synthetic air with a constant flow rate.

Results and discussion

Figure 1(a) shows the x-ray diffraction (XRD) result of the as-cast Zr-based MGs. The curve contains only one broad peak, demonstrating the amorphous nature of the substrate. Figure 1(b) shows the continuous differential scanning calorimeter (DSC) curve with a heating rate of $20\text{ }^{\circ}\text{C min}^{-1}$. As shown in figure 1(b), there is one exothermic peak after reaching $650\text{ }^{\circ}\text{C}$. This corresponds to the sequential phase transition of the amorphous phase to the crystalline phase. The glass transition point T_g occurs at $427\text{ }^{\circ}\text{C}$, and the crystalline point T_x occurs at $495\text{ }^{\circ}\text{C}$. The temperature range of the study is set as $390\text{ }^{\circ}\text{C}$ and $450\text{ }^{\circ}\text{C}$ to observe the complete oxidation behaviors of Zr-based MGs below and above the T_g value.

Figure 2 shows the surface morphologies of Zr-based MGs after oxidation at different temperatures. No white nodules form in the as-cast MGs below T_g , but some white line-like structures become more obvious along the original grinding grooves. After oxidation above T_g , many white nodules are observed on the surface in a uniform distribution (figure 2(b)). For the pre-deformed specimens, the white line-like structures preferentially form along the track of prefabricated shear bands below T_g , and numerous white nodules form along the grooves of shear bands above T_g . The shear bands observed around the indents are the shear offsets along the shear plane. These surface imperfections may provide easier nucleation sites for oxidation [21, 22]. Therefore, the preferential oxidation on the shear bands may be attributed to microstructural change at the surface due to the appearance of shear bands. The oxidation features of the fully crystalline alloy are also investigated for comparison. The specimens are annealed in vacuum to reach a fully crystalline state. As shown in figures 2(e) and (f), no oxides are found on the smooth surface at both $390\text{ }^{\circ}\text{C}$ and $450\text{ }^{\circ}\text{C}$, which means that the fully crystalline state has better oxidation resistance than the as-cast and pre-deformed states.

Figure 3 shows the corresponding XRD patterns of oxide phases formed at different temperatures. Before T_g , tetragonal ZrO_2 ($t\text{-ZrO}_2$) are found after oxidation in the as-cast samples. The formation of $t\text{-ZrO}_2$ is commonly seen in the oxidation process of Zr-based MGs. However, a broad peak still can be observed from the XRD pattern which could be due primarily to the slow nucleation and growth of the oxides at this temperature. At

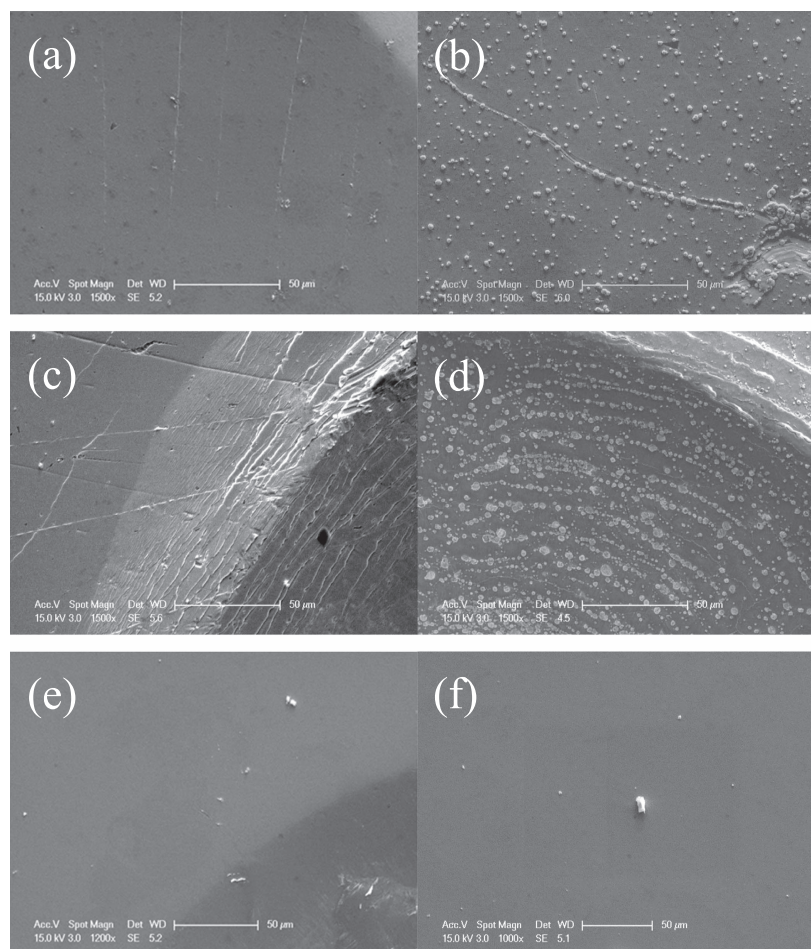


Figure 2. SEM images showing the oxidation features of the Zr-based MGs: (a) and (b) the as-cast specimens oxidized at 390 °C and 450 °C, respectively; (c) and (d) the pre-deformed specimens oxidized at 390 °C and 450 °C, respectively; (e) and (f) the fully crystallized specimens oxidized at 390 °C and 450 °C, respectively.

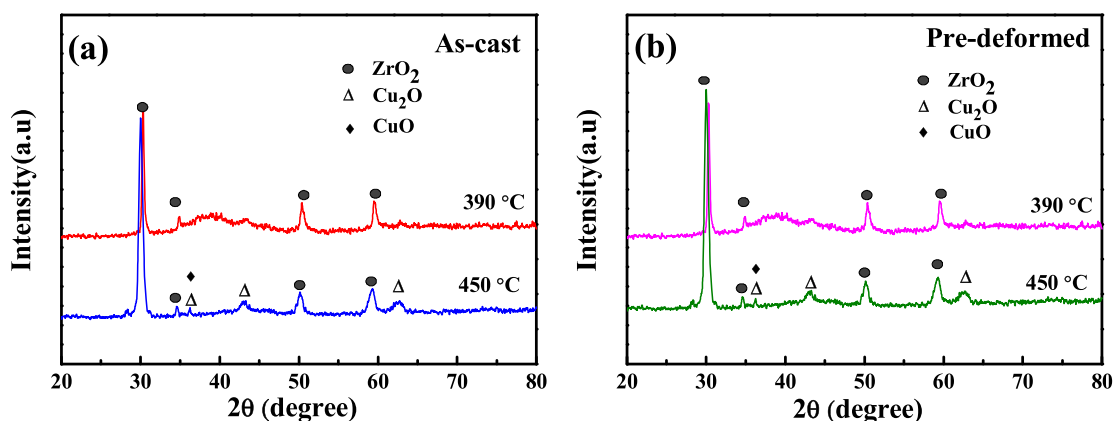


Figure 3. XRD curves of the (a) as-cast and (b) pre-deformed Zr-based MGs oxidized at 390 °C and 450 °C.

450 °C, except for the major *t*-ZrO₂ phase, minor amounts of Cu₂O and CuO phases are observed. The oxidation products of pre-deformed MGs are similar to those of as-cast ones except for the increased intensity of *t*-ZrO₂ phase. Actually, the XRD patterns cannot provide the detailed structural and chemical information on the growing oxides owing to the limited resolution.

Figure 4 shows the square of mass change curves as a function of the time of oxidation duration for the as-cast Zr-MGs and their pre-deformed and crystallized counterparts. The oxidation kinetics of crystalline alloy follows a single parabolic-rate law with a constant oxidation rate K_p . However, more complex kinetics is

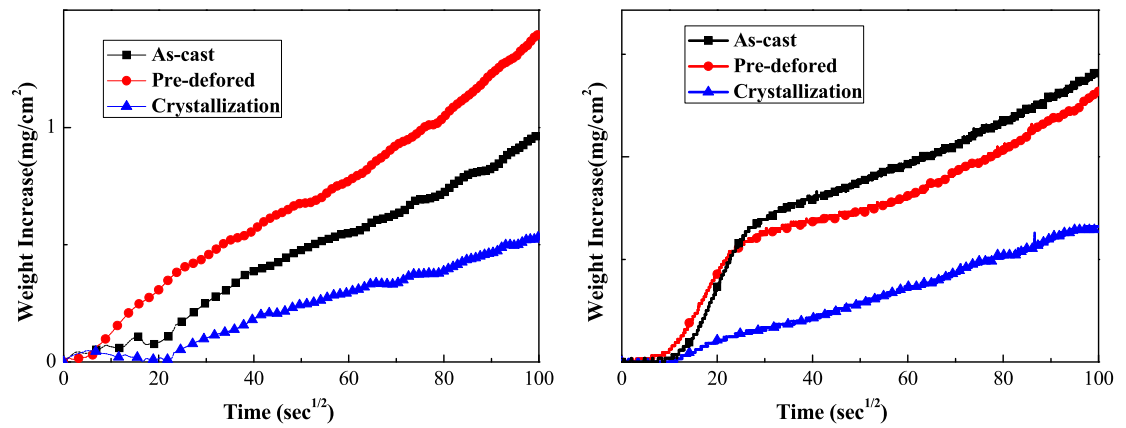


Figure 4. Plots of the mass gain (mg/cm²) versus the square root of time (s^{1/2}) for the as-cast, pre-deformed, and crystallized MGs at (left) 390 °C and (right) 450 °C.

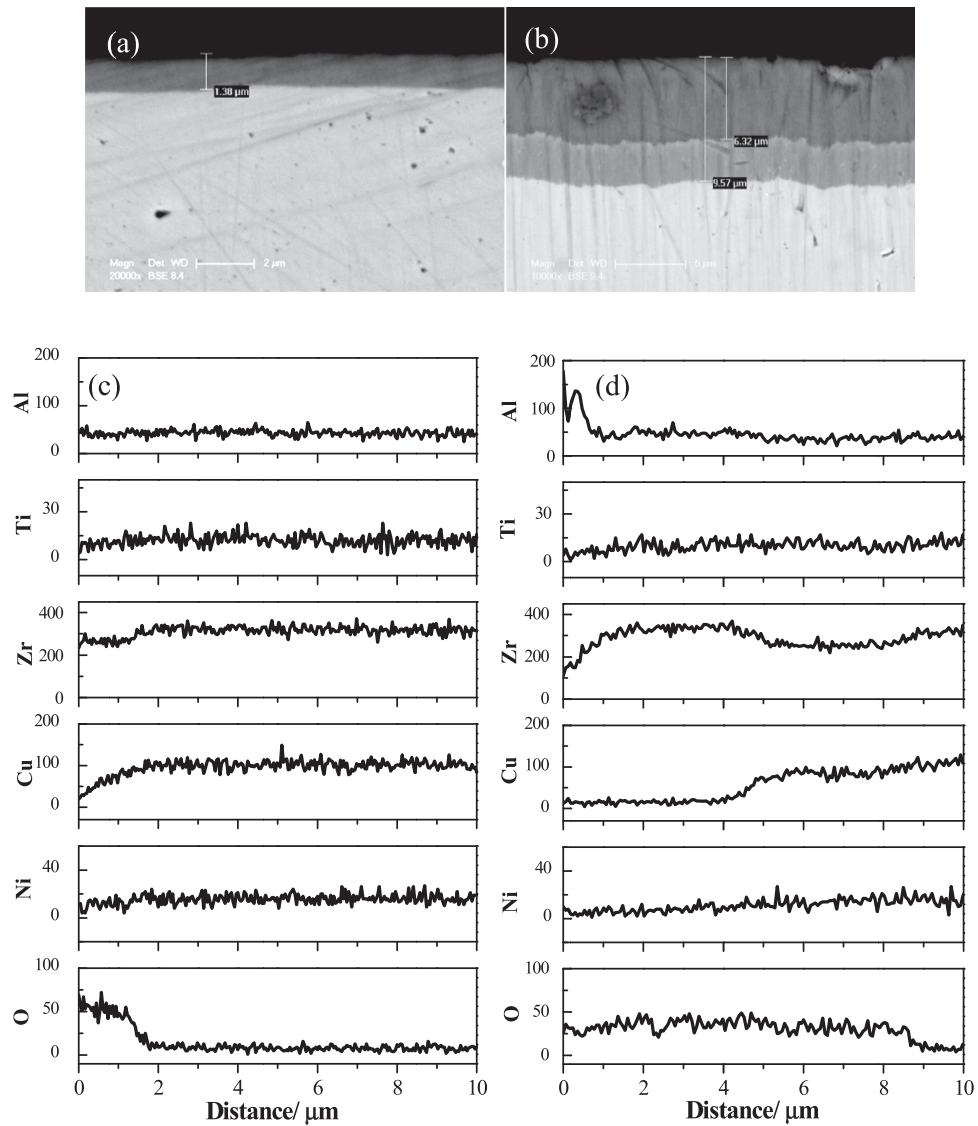


Figure 5. Cross section of the SEM images of the as-cast samples oxidized at (a) 390 °C and (b) 450 °C; corresponding EDS line profiles at (c) 390 °C and (d) 450 °C.

observed for the as-casted and pre-deformed MGs, consisting of an accelerated oxidation rate stage up to about 15 min, followed by a steady-state stage from 15 min to about 3 h. The parabolic-rate constant K_p of the steady-state is calculated as $6 \times 10^{-11} \text{ g}^2/\text{cm}^4/\text{s}$, which is nearly identical to that observed for the crystalline

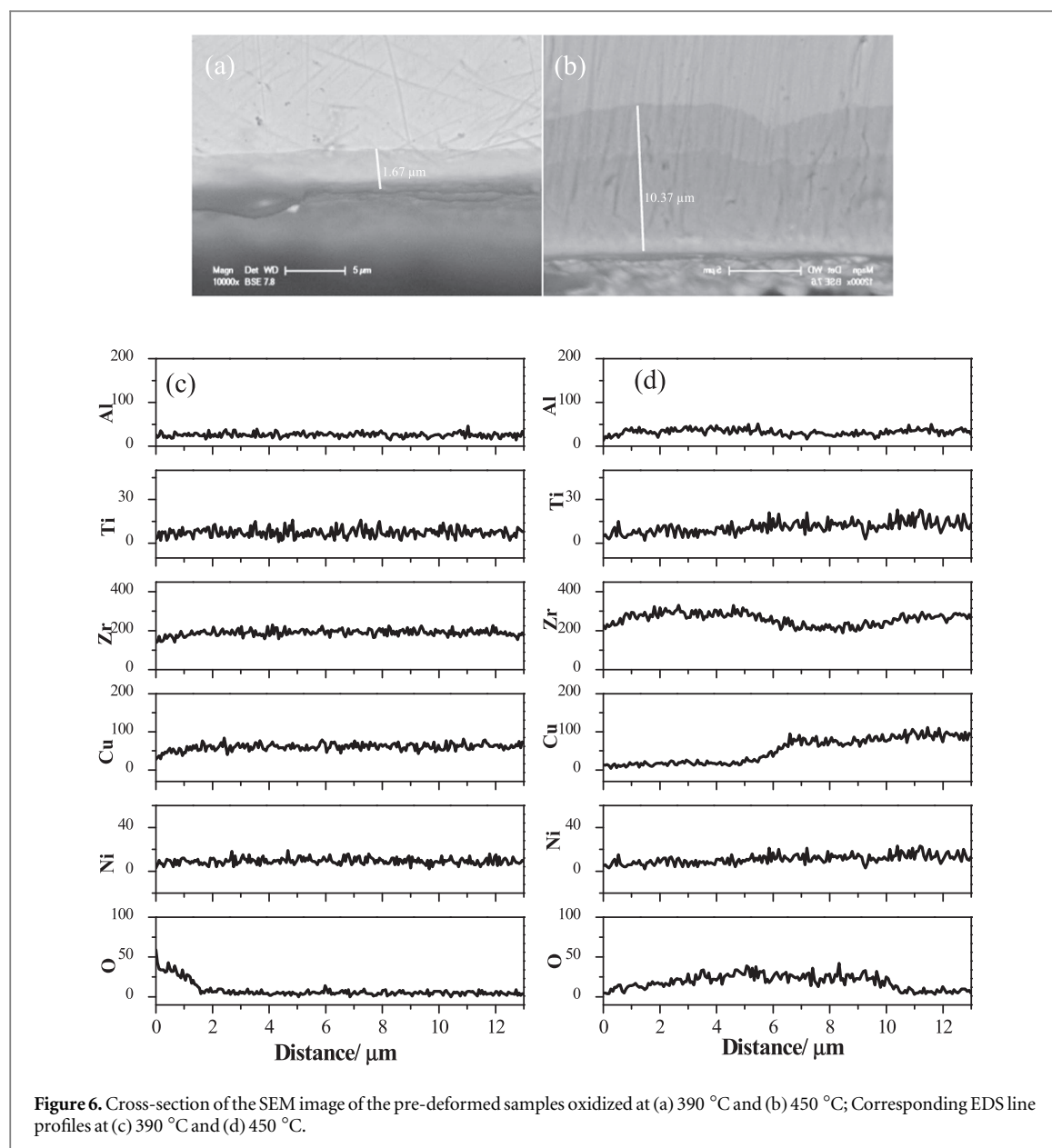
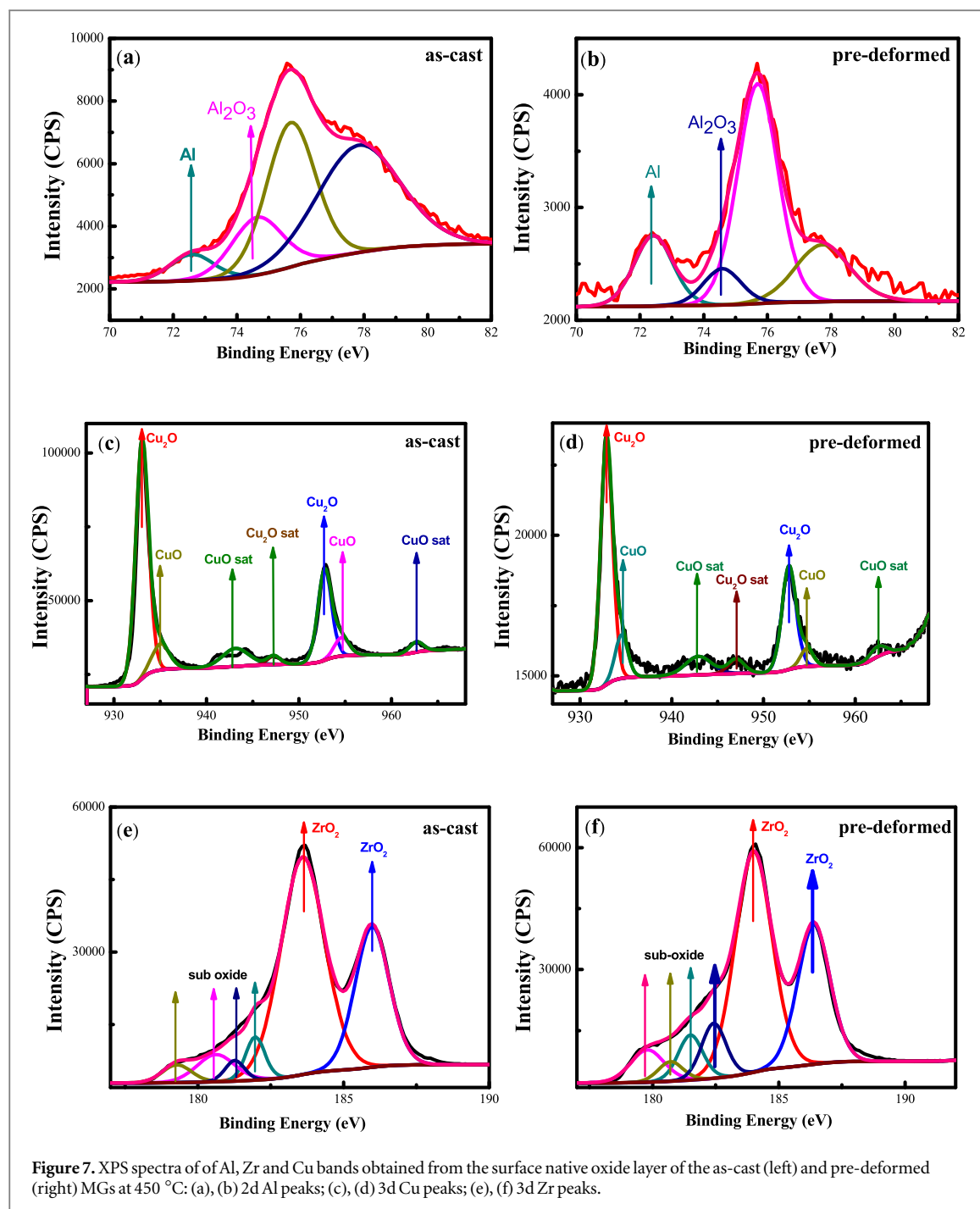


Figure 6. Cross-section of the SEM image of the pre-deformed samples oxidized at (a) 390 °C and (b) 450 °C; Corresponding EDS line profiles at (c) 390 °C and (d) 450 °C.

counterpart, implying that the diffusion mechanism is dominant for the whole reaction. This might be due to crystallization of the amorphous alloy after an extended period of oxidation. Most interesting, pre-deformed treatment can significantly improve the oxidation of MGs in the initial short-term oxidation stage, and the onset of initial oxidation appears earlier than for the as-cast ones.

To examine the oxidation and diffusion mechanism in the Zr-based MGs, the cross section of the oxide scale formed in the as-cast MGs is shown in figure 5, after exposure to air under different thermal conditions for 3 h. As shown in figure 5, the thickness of the formed oxide scale was about 1.38 μm below T_g , and 9.57 μm above T_g . Two different oxide layers formed above T_g , corresponding to the above-mentioned diffusion-controlled oxidation behavior, and probably due to a mismatch in the thermal expansion coefficients between the outer and inner oxide scales.

Figures 5(c) and (d) show the concentration depth profiles of the oxidized MGs at different temperatures. The concentrations of Zr and Cu show similar distribution with depth in the oxide layer below T_g , and the oxidation products may correspond to ZrO_2 and oxide of copper [23]. The concentrations of other elements exhibit a slight change with depth. Previous studies showed deteriorated oxidation resistance of Zr-based MGs with the addition of Cu [24]. This oxide layer forms because Zr and Cu are present at high concentration and has high oxidative activity, allowing the oxidation of the binary Zr-Cu MGs even at room temperature [19]. However, this is not true above T_g . As shown in figure 5(d), Al diffuses predominantly outward and spreads over the outermost oxide surface. Because Al ions have the smallest ionic radii, the sample surface undergoes rapid and preferential oxidation of Al during the initial period, with the near surface predominately consisting of



Al_2O_3 . This Al oxide layer is so dense that it can limit the migration and diffusion of other ions towards O ions, resulting in an enriched Al layer at the surface.

Al plays a dominant role in the oxidation process of as-cast MGs. There is a great deal of research interest in investigating pre-deformed MGs, in which a distinct oxidation response may occur due to pre-existing shear bands in the surface. Figure 6 shows the cross section and EDS line profile of the oxide scale formed during oxidation of pre-deformed MGs. The thickness of the oxide scale is estimated to be about 1.67 μm and 10.37 μm below and above T_g , which is slightly larger than the thickness in as-cast MGs. An obvious separated oxide layer is also observed above T_g . However, a different oxidation mechanism is observed in the pre-deformed MGs compared to that in the as-cast ones, where the Al-rich oxidation layer does not appear in the outermost oxide surface. The diffusion of other ions is enhanced, as shown in figure 6(d).

In order to investigate the oxidation states of the constituent elements in the native oxide layer, surface XPS analyses of the as-cast and pre-deformed Zr-based MGs at 450 °C are conducted [25–27]. The XPS spectra are shown in figure 7 and these data are summarized in table 1. As shown in table 1, Al in the native oxide layer of as-cast MGs has its highest oxidation state and forms Al_2O_3 . Only a minor fraction of metallic Al (about 28.6%) can

Table 1. Chemical composition of the native oxide layer on the MG surface measured by XPS, C^t denotes total content of the elements in the native oxide layer; C^p denotes the partial content of different compounds.

	As-cast		Pre-deformed	
	C^t , %	C^p , %	C^t , %	C^p , %
Al	22.2	Al	9.11	Al
		Al₂O₃		Al₂O₃
Zr	42.72	Sub-oxide	81.35	Sub-oxide
		ZrO₂		ZrO₂
Cu	32.47	CuO	5.92	CuO
		Cu₂O		Cu₂O

be present. Most of Zr atoms (i.e. 65 at%) are oxidized forming ZrO₂ phase. A small amount of Zr atoms (i.e. 35 at%) is found to be in the form of sub oxide states. About half of Cu atoms (i.e. 58 at%) are connected in Cu₂O compound. The other half of Cu atoms (i.e. 42 at%) correspond to CuO compound. As also shown in table 1, the fraction of Al in the native oxide layer of as-cast MGs is about 22.2%, which is much larger than that in unoxidized as-cast MGs. It demonstrates that Al may act as a scavenger for both absorbed and intrinsic oxygen [28]. After pre-deformed treatment, the total Zr content in the upper layer increases with the decrease of Al and Cu. The phenomenon correlates well with the formation of a Zr-depleted region at the oxide-metallic glassy matrix interface: Zr migrates to the oxide while Cu diffuses towards metallic glassy phase, which results in the formation of the obvious separated oxide layer as shown in figures 5 and 6. That is to say, the diffusion of Zr and Cu in MGs is enhanced owing to the pre-deformed treatment, which agrees well with our previous assumptions.

Actually, the MGs could be viewed as tightly bonded atomic clusters that overlap to form the percolating 'skeleton' of the glassy structure, with loosely bonded free-volume regions when subjected to the pre-deformed treatment [29]. The formed oxide layer is defective due to the local increase in free volume and the significant shear-induced dilation in MGs. The easy migration of Zr- and Cu-ion is possible through the loose free-volume regions. Thus, the local increase in the free volume and significant shear-induced dilation of the local structure may explain the accelerated inward diffusion of other elements.

Conclusion

In this study, the oxidation behaviors of the as-cast, pre-deformed, and crystallized Zr-based MGs were explored near the glass transition point. The oxidation kinetics of the crystallized MGs followed a parabolic-rate law, and the as-cast and pre-deformed MGs exerted a typical two-stage behavior above T_g . Many white nodules were observed on the as-cast and the pre-deformed MGs above T_g . Pre-deformed treatment significantly improved the oxidation rate of MGs, in which the onset of initial oxidation occurred earlier than for the as-cast ones. The Al element acted as a preferred scavenger that absorbed intrinsic oxygen in the near-surface of as-cast MGs, with no effect in the pre-deformed MGs. We speculated that the local increase in free volume and significant shear-induced dilation of the local structure in MGs may be the reason for the accelerated diffusion of other elements.

Acknowledgments

The authors would like to acknowledge the support by the National Natural Science Foundation of China (Grant Nos.51401028, 51271193, 11402277) and the Strategic Priority Research Program of the Chinese Academy of Sciences (Grant No. XDB22040303).

ORCID iDs

Kun Zhang  <https://orcid.org/0000-0003-0997-0428>

References

- [1] Inoue A and Zhang T 1996 Fabrication of bulk glassy Zr₅₅Al₁₀Ni₅Cu₃₀ alloy of 30 mm in diameter by a suction casting method *Mater. Trans. JIM* **37** 185–7
- [2] Greer A L and Ma E 2007 Bulk metallic glasses: at the cutting edge of metals research *MRS Bull.* **32** 611–9

- [3] Wang W H *et al* 1999 Elastic constants and their pressure dependence of $Zr_{41}Ti_{14}Cu_{12.5}Ni_9Be_{22.5}C_1$ bulk metallic glass *Appl. Phys. Lett.* **74** 1803–5
- [4] Xu D *et al* 2004 Bulk metallic glass formation in binary Cu-rich alloy series $Cu_{100-x}Zr_x$ ($x = 34, 36, 38.2, 40$ at%) and mechanical properties of bulk $Cu_{64}Zr_{36}$ glass *Acta Mater.* **52** 2621–4
- [5] Wang G Y *et al* 2004 Fatigue behavior of bulk-metallic glasses *Intermetallics* **12** 885–92
- [6] Peter W H *et al* 2002 Localized corrosion behavior of a zirconium-based bulk metallic glass relative to its crystalline state *Intermetallics* **10** 1157–62
- [7] Amiya K *et al* 1994 Mechanical strength and thermal stability of Ti-based amorphous alloys with large glass-forming ability *Materials Science and Engineering: A* **179** 692–6
- [8] Zhang T and Inoue A 1998 Thermal and mechanical properties of Ti-Ni-Cu-Sn amorphous alloys with a wide supercooled liquid region before crystallization *Mater. Trans. JIM* **39** 1001–6
- [9] Jun H J, Lee K S and Chang Y W 2010 Deformation behavior and formability of a Ti-Zr-Ni-Be bulk metallic glass within supercooled liquid region *Intermetallics* **18** 1537–43
- [10] Carmo M *et al* 2011 Bulk metallic glass nanowire architecture for electrochemical applications *ACS Nano* **5** 2979–83
- [11] Kim S Y *et al* 2013 Capillary flow of amorphous metal for high performance electrode *Sci. Rep.* **3** 2185
- [12] Lim K R *et al* 2014 Oxidation induced amorphous stabilization of the subsurface region in Zr-Cu metallic glass *Appl. Phys. Lett.* **104** 031604
- [13] Wei G and Cantor B 1988 The oxidation behaviour of amorphous and crystalline $Fe_{78}Si_9B_{13}$ *Acta Metall.* **36** 2293–305
- [14] Cocke D L *et al* 1988 The oxidation behavior of amorphous and polycrystalline Zr-Ni alloys *Materials Science and Engineering* **99** 497–500
- [15] Kai W *et al* 2009 Air oxidation of a $Zr_{58}Cu_{22}Al_{12}Fe_8$ bulk metallic glass at 350 °C–550 °C *J. Alloys Compd.* **483** 519–25
- [16] Tam C Y and Shek C H 2005 Oxidation behavior of $Cu_{60}Zr_{30}Ti_{10}$ bulk metallic glass *J. Mater. Res.* **20** 1396–403
- [17] Hsieh H H *et al* 2004 Effect of Zr-content on the oxidation and phase transformation of Zr-based amorphous alloys in air *Intermetallics* **12** 1089–96
- [18] Wu Y, Nagase T and Umakoshi Y 2006 Effect of crystallization behavior on the oxidation resistance of a Zr-Al-Cu metallic glass below the crystallization temperature *J. Non-Cryst. Solids* **352** 3015–26
- [19] Kim C W, Jeong H G and Lee D B 2008 Oxidation of $Zr_{65}Al_{10}Ni_{10}Cu_{15}$ bulk metallic glass *Mater. Lett.* **62** 584–6
- [20] Greer A L, Cheng Y Q and Ma E 2013 Shear bands in metallic glasses *Materials Science and Engineering: R: Reports* **74** 71–132
- [21] Vianco P T and Li J C M 1987 Annealing of shear bands in metallic glasses *J. Mater. Sci.* **22** 3129–38
- [22] Pampillo C A 1972 Localized shear deformation in a glassy metal *Scr. Metall.* **6** 915–7
- [23] Hu Z *et al* 2011 Oxidation features of plastic deformed Zr-based bulk metallic glass *J. Alloys Compd.* **509** S69–73
- [24] Toma D, Meuris M and Koster U 1999 Oxidation of Zr-based metallic glasses in air *J. Non-Cryst. Solids* **250** 719–23
- [25] Koster U and Jastrow L 2007 Oxidation of Zr-based metallic glasses and nanocrystalline alloys *Materials Science and Engineering: A* **57–62** 449–51
- [26] Louzguine-Luzgin D V, Chen C L, Lin L Y, Wang Z C, Ketov S V, Miyama M J, Trifonov A S, Lubchenko A V and Ikuhara Y 2015 Bulk metallic glassy surface native oxide: its atomic structure, growth rate and electrical properties *Acta Mater.* **97** 282–90
- [27] Lim K R, Kim W T and Kim D H 2012 Characterization of the oxide layer formed on the Cu-Zr based metallic glass during continuous heating *Appl. Microscopy* **42** 174
- [28] Heinrich J, Busch R and Muller F 2012 Role of aluminum as an oxygen-scavenger in zirconium based bulk metallic glasses *Appl. Phys. Lett.* **100** 071909
- [29] Ye J C *et al* 2010 Atomistic free-volume zones and inelastic deformation of metallic glasses *Nat. Mater.* **9** 619–23